Geophysical Research Letters®

Key Points:

- First fine-scale 3D images reveal an interconnected rift plumbing system using scattering and absorption mapping
- High scattering and absorption mark fluid-filled faults that degas magmatic fluids and act as potential conduits for carbonatite melts
- A high absorption melt reservoir feeds eruptions at Oldoinyo Lengai and dike intrusions and acts as a transfer zone between rift segments

Supporting Information:

Supporting Information may be found in the online version of this article.

Correspondence to:

M. C. Reiss,
reiss@geophysik.uni-frankfurt.de

The Interconnected Magmatic Plumbing System of the Natron Rift

M. C. Reiss[1] , **L. De Siena[2]** , and **J. D. Muirhead[3]**

[1]Goethe-Universität Frankfurt, Institut für Geowissenschaften, Frankfurt, Germany, [2]Institut für Geowissenschaften, Johannes Gutenberg Universität Mainz, Mainz, Germany, [3]School of Environment, University of Auckland, Auckland, New Zealand

Abstract Understanding the magmatic plumbing system of rift volcanoes is essential when examining the interplay between magmatic and tectonic forces. Recent seismicity, volcanic activity, magma emplacement, and volatile release make the Natron basin the ideal location to study these processes in the East African Rift System. Here, we present the first high-resolution tomographic imaging of Oldoinyo Lengai volcano and surrounding volcanic systems using attenuation mapping. High scattering and absorption features reveal fluid-filled fracture networks below regions of magmatic volatile release at the surface and a close spatial association between carbonatite volcanism and deeply penetrating, fluid-filled faults. High-absorption features appear sensitive to fluids and thermal gradients, revealing a central sill complex and connected plumbing system down to the mid-crust, which links volcanoes and rift segments across the developing magmatic rift.

Plain Language Summary The interplay between magmatic and tectonic forces during rifting is still debated. While they are a key component of rift development, the complex structures of rifts and melt storage systems scatter and absorb seismic waves passing through them: in turn, this deteriorates the quality of the subsurface images we obtain from them. In this study, we use the loss of energy suffered by seismic waves to image the Natron basin, which hosts extinct volcanoes and the only active natrocarbonatite volcano on Earth, Oldoinyo Lengai. The results identify areas of melt storage and fracture networks that feed volatiles and melt to this volcano. Results suggest that carbonatite melts may ascend through the crust efficiently along deep-seated faults systems, while silicate melts in the region may be primarily sourced from a separate melt reservoir. This reservoir, which is elongate and oriented oblique to the general trend of the rift, may act as a magmatic transfer zone between two rift segments.

1. Introduction

A key questions in the dynamics of rifting is the extent to which it is controlled by magmatic and tectonic processes, and how their control varies during the rift evolution (Ebinger & Casey, 2001; Marzen et al., 2020; Muirhead et al., 2016; Thybo & Nielsen, 2009). While slip on large-scale border faults is sometimes dominant during the onset of rifting, a steady supply of melt increases the likelihood of extensional strain accommodation via magmatic processes, such as dike intrusions (Buck, 2004; Keir et al., 2006; Muirhead et al., 2016). In turn, these can initiate shallow upper crustal faulting (Rowland et al., 2007; Rubin & Pollard, 1988; Trippanera et al., 2019). The release of magmatic volatiles weakens the lithosphere through increased pore fluid pressures (Reyners et al., 2007; Sibson, 2000) and/or hydration and mineral reactions (Moore & Rymer, 2007), ultimately assisting in strain localization and break up of thick strong lithosphere (Ebinger & Casey, 2001; Muirhead et al., 2016).

The Natron basin of the East African Rift System is the ideal place for exploring the interplay between magmatic and tectonic processes during the earliest stages (<5 Myr) of magmatic continental rifting (Biggs et al., 2013; Calais et al., 2008; Muirhead et al., 2015; Oliva et al., 2022; Roecker et al., 2017; Weinstein et al., 2017). Magmatic and volatile weakening here have been previously illustrated through analysis of seismicity patterns (Albaric et al., 2014; Oliva et al., 2019; Reiss et al., 2021; Weinstein et al., 2017), geophysical imaging (Roecker et al., 2017; Tiberi et al., 2019), and analysis of faulting patterns and regions of mantle volatile discharge (Lee et al., 2016, 2017; Muirhead et al., 2016, 2020). We present the first high-resolution 3D absorption and scattering images in this region, which show how melt and other fluids are distributed from mid-crustal depths to Oldoinyo Lengai, faults and regions of potentially active dike and sill intrusions.

a)

b)
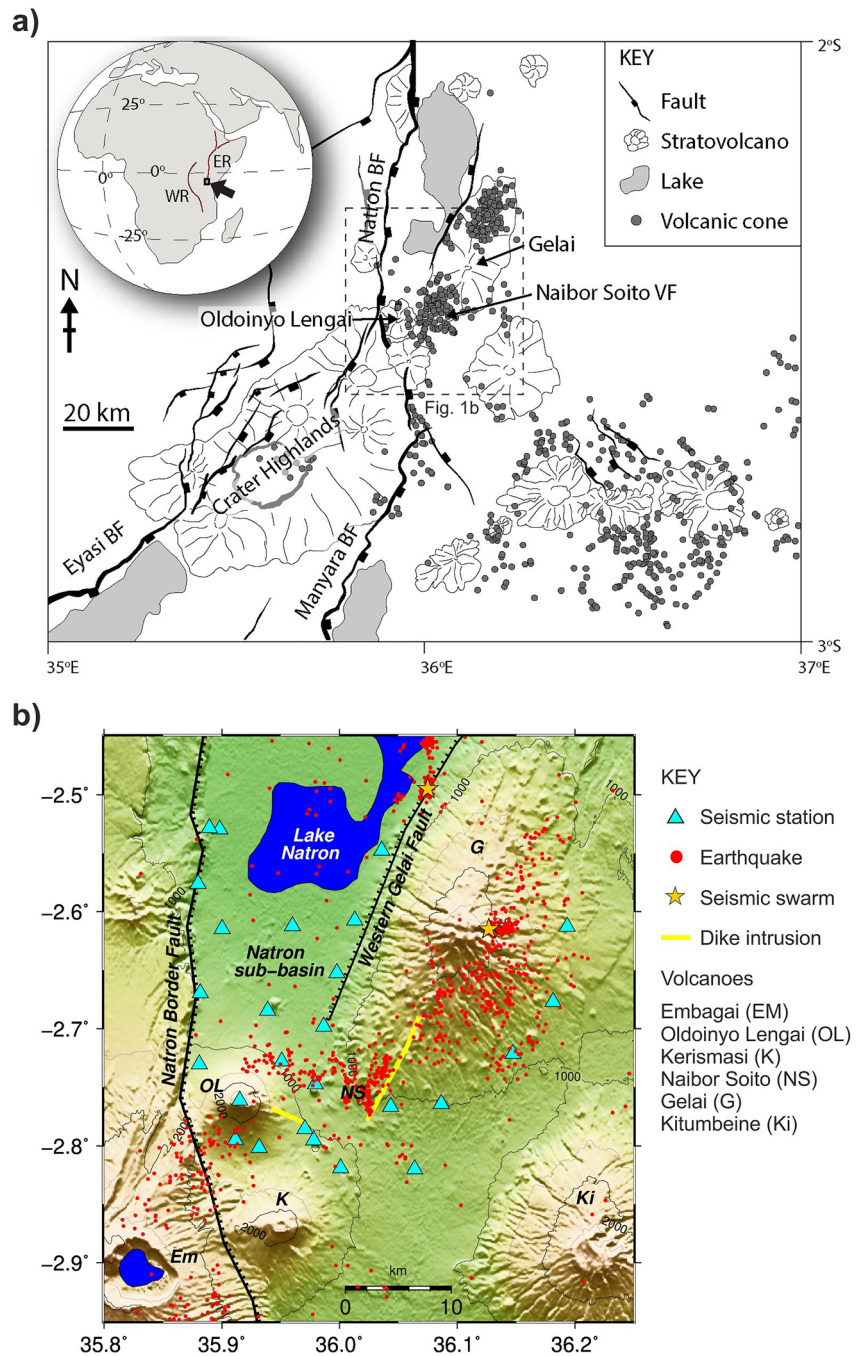
Figure 1. Map of the research area located in the East African Rift (inset). (a) Tectonic map with volcanoes and faults. The dashed line denotes the area in Figure 1b. (b) Topographic map with earthquakes used for the inversion (Reiss et al., 2021).

2. Volcano-Tectonic Setting of the Natron Basin

The Natron basin is part of the North Tanzanian Divergence, an up to ~300 km-wide zone that includes the Ngorongoro-Kilimanjaro Volcanic diachronous belt, formed since ~6 Ma, and the Natron, Eyasi, Manyara and Pangani rift basins (Le Gall et al., 2008; Mana et al., 2015; Muirhead et al., 2015, Figure 1a). The North Tanzanian Divergence is part of the East African Rift System, the longest continental rift worldwide. Slow extension rates, typically between 1 and 2 mm yr^{-1} characterize rifting in the Natron basin today (Saria et al., 2014). Here, faulting initiated at ~3 Ma (Foster et al., 1997): the largest active structures are the Natron border fault,

which bounds the western side of the modern basin, and the ∼50 km-long Western Gelai fault on the western flanks of Gelai volcano (Figure 1b). The sub-basin between both faults has a maximum sediment fill of 3.3 km and is underlain by Proterozoic or Archean rocks (Ebinger et al., 1997). Deformation processes in the Natron basin are presently assisted by fluids rising through the plate (Albaric et al., 2014; Lee et al., 2016; Muirhead et al., 2020; Reiss et al., 2021; Weinstein et al., 2017). The Natron basin also includes the only active natrocarbonatite volcano on Earth, Oldoinyo Lengai. This volcano is adjacent to the border fault at the southern end of the Natron basin (Figure 1) and is bordered to the east by the Naibor Soito volcanic field, a monogenetic cone field with erupted deposits known for their abundance of metasomatized mantle xenoliths (Aulbach et al., 2011; Dawson et al., 1995; Muirhead et al., 2015; Figure 1). The volcanic centers of the Naibor Soito volcanic field have erupted both adjacent to and on top of the ∼1 Ma old Gelai volcano (Mana et al., 2015).

The oldest volcanic deposits at Oldoinyo Lengai are dated at ∼0.37 Ma (Sherrod et al., 2013), and the volcano shows alternating episodes of silicate explosive eruptions and effusive natrocarbonatite eruptions (Dawson et al., 1995; Kervyn et al., 2010; Sherrod et al., 2013). The most recent explosive eruption sequence in 2007–2008 was preceded and accompanied by a July-September 2007 earthquake swarm (70 earthquakes with $M > 4$) below the Naibor Soito volcanic field and inactive Gelai volcano (Baer et al., 2008; Biggs et al., 2009, 2013; Calais et al., 2008; Kervyn et al., 2010). Field and InSAR observations of these events showed extensive surface deformation, best explained by slip on a normal fault followed by dike-opening (Biggs et al., 2009, 2013; Calais et al., 2008; Jones et al., 2019). A second diking event ∼3.4 km below Oldoinyo Lengai occurred between October and December 2007 (Biggs et al., 2013). Observation and modeling of InSAR data shows that both events are best explained by the emptying of a shallow magmatic reservoir near the respective dikes (Biggs et al., 2009, 2013; Calais et al., 2008). Based on petrological observations, magma volume estimates and stress calculations, a single shallow magmatic reservoir could not have sourced both the 2007 eruption at Oldoinyo Lengai and the dike intrusions (Biggs et al., 2013; Kervyn et al., 2010). This volcano-tectonic event was most likely triggered by an over-pressurized deep magma reservoir, and magma was then distributed from there throughout the shallow crust (Baer et al., 2008; Biggs et al., 2013).

3. Methods

When a seismic wave travels through the crust, it loses energy by geometrical spreading, scattering and absorption, which gives the total attenuation of the wave. Attenuation mechanisms can be separated using different parts of seismograms recorded from local or regional seismicity. The peak-delay ($\log_{10}$Tpd, the delay time of the direct S-wave onset to the maximum amplitude of a seismogram's envelope) is a marker of forward scattering from small-scale velocity perturbations after correcting for path propagation (Calvet et al., 2013; Takahashi et al., 2007). The coda of high-frequency seismograms can enter the diffusive regime at long lapse times from the earthquake origin in a uniform anisotropic half-space. Coda attenuation (Qc^{-1}), which is measured from the exponential decay of the envelope with time (Aki & Chouet, 1975), thus measures seismic absorption (Calvet et al., 2013; Shapiro et al., 2000).

Absorption tomography does not require an underlying velocity model, but is based on the primary assumption that diffusion onsets after a specific lapse time (De Siena et al., 2017; Mayor et al., 2016; Vargas et al., 2019). At high frequencies, these assumptions are fulfilled quickly within volcanic media (Del Pezzo & Ibáñez, 2020; Wegler & Lühr, 2001). The sensitivity of absorption measurements to space can be defined using 3D multiple-scattering sensitivity kernels (Del Pezzo & Ibáñez, 2020; Del Pezzo et al., 2018; Zhang et al., 2021), allowing to set up averaging or inverse problems (Akande et al., 2019; Del Pezzo & Ibáñez, 2020; Shito et al., 2020). Here, we use MuRAT3.0, an open access code that measures peak delays and coda attenuation and inverts them in space using regionalization and coda sensitivity kernels.

We use the seismic data of 26 stations and the earthquake catalog by Reiss et al. (2021, Figure 1b). From the catalog, we selected 1071 local earthquakes with magnitudes in the range $M_L = 0.5$–3.6 (Table S1). Waveforms used in the inversion fulfill the following criteria: (a) a signal-to-noise ratio of the P-wave onset on the vertical component >2.5; (b) both P- and S-wave picks; (c) the earthquake was recorded at ≥ five stations; and (d) the earthquake is located within an inversion volume of 3 km to −21 km in altitude, [−2.95°, −2.45°] latitude, and [35.8°, 36.25°] longitude. Selecting this volume removes the trade-off produced by earthquakes far from the

array, which have greater location uncertainties. We describe our choices of inversions parameters, filters and resolution tests in Text S1 of Supporting Information S1.

The separation and mapping of different attenuation mechanisms allows for discrimination between tectonic (e.g., faults and fractures) and magmatic- and fluid-related structures (e.g., dikes, sills, and fluid-filled fractures; De Siena et al., 2016; Napolitano et al., 2020). Peak delays have been used previously as a marker of scattering attenuation, mapping intrusions of mantle or lower-crustal material within mountain ranges (Calvet et al., 2013), and are especially effective at detecting volcanic centers at the regional scale (Takahashi et al., 2007) and large individual faults in volcanic regions (De Siena et al., 2016; Gabrielli et al., 2020; Zieger et al., 2016). The primary cause for absorption is grain boundary friction in dry rocks. In (partially) saturated, porous rocks, the mechanisms depend both on frequency and fluid flow and fluid-rock interactions (Tisato & Madonna, 2012). Scattering and absorption mappings have extensively been used to study the plumbing systems of volcanoes (Akande et al., 2019; De Siena et al., 2016, 2017; Prudencio et al., 2018); however, this study represents the first application of 3D scattering and absorption mapping in a magmatic rift setting.

4. Results and Discussion

We present $\log_{10}Tpd$ and Qc^{-1} results for 9, 12, 15 and 18 Hz above 15 km depth. Joint maps of scattering and absorption are obtained separating the spatial $\log_{10}Tpd(f)$ versus $Qc^{-1}(f)$ into their parameter space, after removing the mean computed over all parameters (De Siena et al., 2016). To emphasize the most important results, we show selected horizontal and vertical cross-sections in the main text, while results for all frequencies are shown as four horizontal cross sections in the supplements (Figures S8–S10 in Supporting Information S1).

4.1. Fluid Transport Along Large-Scale Faults

Both major faults in the Natron basin (Natron border and Western Gelai faults, Figure 1b) show different attenuation mechanisms at different depths and frequencies. The Natron border fault is characterized by strong scattering above 6 km for higher frequencies (Figure 2a), while high scattering below 6 km only marks its southern, more seismically active segment (Figure 2b, Reiss et al., 2021; Weinstein et al., 2017). At 6 km and 9 Hz, the fault shows both high scattering and absorption (HAS) south of Oldoinyo Lengai. A spike test for Qc^{-1} reveals that while we have resolution at this particular depth/frequency in this area, we only have good resolution from 14 km depth to the surface and along the length of the fault for higher frequencies (Figure S11 in Supporting Information S1). Considering a vertical cross-section along the border fault at 15 Hz (Figure 2d), we find that the fault shows HAS from 12 km to the surface and a slight southward trend with depth. The Western Gelai fault shows high absorption at lower frequencies down to depths of 10 km (Figures 3a and 3b) and a HAS feature in the northern part of the fault for all frequencies at 6 km (Figure 2b). This is the area encompassed by the 10 October 2019 seismic swarm identified by Reiss et al. (2021).

HAS is a demonstrated marker of fluid-filled fracture networks at high frequencies, which can be continuously reactivated by distant seismicity and remain unhealed (Napolitano et al., 2020). The presence of gas bubbles produce some of the highest scattering and absorption responses at the laboratory and volcanic field scales (De Siena et al., 2017; Tisato et al., 2015). Studies have shown that both faults are associated with fluid transport: The Western Gelai fault degasses mantle-derived CO_2 and helium likely sourced from deeper magmatic bodies, which is transported to the surface via deep-reaching faults, while the Natron border fault also releases volatiles that exhibit magmatic mantle signatures (Lee et al., 2016, 2017; Muirhead et al., 2016). Though fluids have long been suspected to play a pivotal role in the triggering of earthquake swarms, the HAS patterns image these fluids and provide evidence for potential fluid-driven fracturing along both faults.

4.2. An Interconnected Magmatic System

Within the central magmatic system, we observe the following features which we will discuss in this order: (a) down to 6 km, we observe strong scattering from Oldoinyo Lengai, to Naibor Soito, to the southern flank of Gelai (Figure 2a); (b) at 6 km depth, the parameter maps reveal several HAS features, from the Natron border fault to Gelai (Figure 2c); (c) at ~8–12 km depth, we see a large high-absorption feature south of Oldoinyo Lengai to Gelai (Figures 3b and 3c); and (d) the core of Gelai exhibits low scattering and absorption (Figures 2c and 3a).
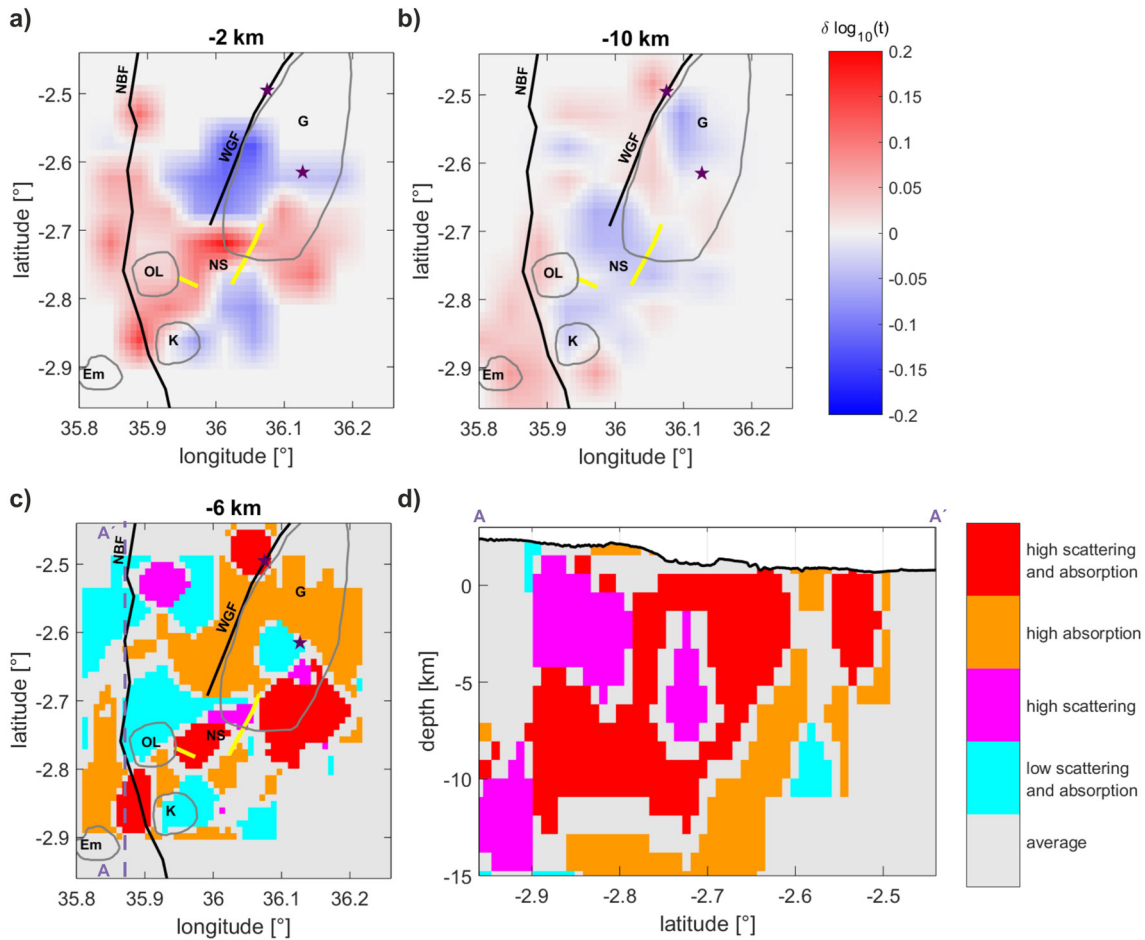
Figure 2. Cross-sections through scattering models and parameter space. Faults are shown as thick black lines: NBF, Natron border fault; WGF, Western Gelai fault. Outlines of the volcanoes and dikes reported in Figure 1b are indicated by yellow and gray lines, respectively. (a and b) Horizontal cross-sections for peak delay for 15 Hz at 2 and 10 km. The color bar is fixed at ±0.2. (c) Horizontal cross-section of parameter map for 9 Hz. (d) Vertical cross-section of parameter map for 15 Hz along the dotted line in (c).

The high scattering from Oldoinyo Lengai to the southern flank of Gelai (Figure 2a and Figure S8 in Supporting Information S1) is in strong contrast to the syn-rift basin. Low scattering here likely reflects the Archean to Protoerzoic basement rock. As both the Natron sub-basin and subsurface beneath Oldoinyo-Naibor Soito-Gelai are subject to extensional normal faulting and we expect faults to be distributed throughout the basin, the comparatively higher scattering features within the central plumbing cannot be explained by the presence of faults alone (Muirhead et al., 2015; Reiss et al., 2021). The Oldoinyo Lengai-Naibor Soito-Gelai system experiences frequent upper crustal diking (Biggs et al., 2013; Calais et al., 2008; Muirhead et al., 2015), and thus we suggest the high scattering more likely reflects a multitude of shallow (<6 km depth), cooled dike intrusions that have pervaded this part of the basin in the last ∼1 Myr (Figure 4).

Directly underneath, HAS patterns support the presence of an active network of fluid- and/or melt-filled fractures extending from Oldoinyo Lengai to the southern flanks of Gelai at 6 km depth: at 12 Hz (Figure 2c), the parameter maps reveal two HAS features, one underneath the border fault segment adjacent to Oldoinyo Lengai, and one east of Oldoinyo Lengai below the 2007 dike intrusion. At 12 Hz and above, a HAS pattern below Naibor Soito extends underneath the Gelai dike intrusion (Figures S10b–S10d in Supporting Information S1). The proximity of the observed HAS patterns to both dike intrusions, which were possibly sourced by magmatic reservoirs below the intrusions (Biggs et al., 2009, 2013; Calais et al., 2008), is striking and the HAS patterns may thus represent small batches of melt that are currently distributed throughout the crust.
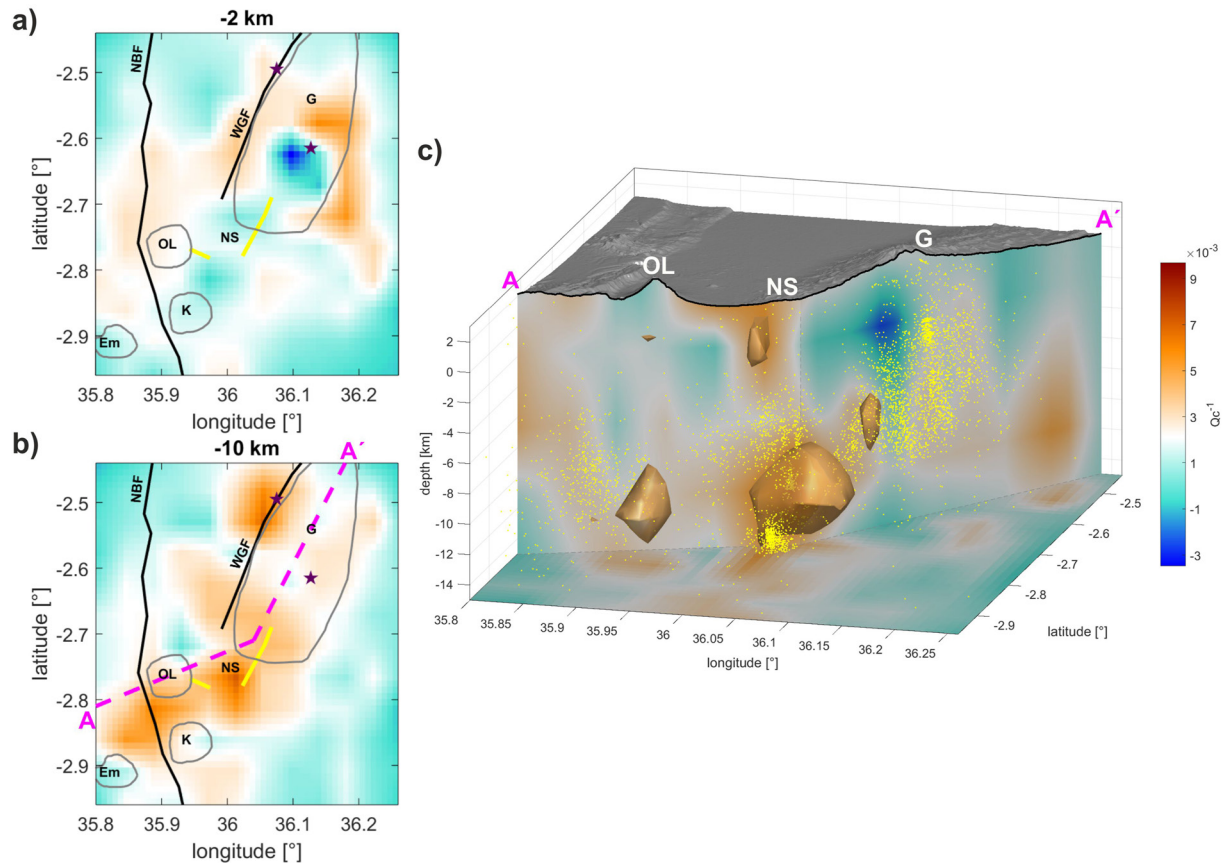
Figure 3. Horizontal and vertical cross-sections of absorption models at different depths and frequencies. The colormaps are asymmetric; the white color denotes the average Qc^{-1}. (a and b) Models for 9 Hz and (c) for 15 Hz. The vertical cross-section in (c) is indicated by the magenta line in (b). Isosurfaces are plotted at 50% of the maximum absorption, earthquakes from Reiss et al. (2021) are yellow dots. Annotations as in Figure 2.

We find evidence that these melt-filled fractures may in turn be fed by a larger magmatic reservoir at greater depth in our absorption models (Figures 3b and 3c). The most consistent high-absorption feature extends from south of Oldoinyo Lengai to Gelai, between ∼8 and 12 km depth, and is delineated as an isosurface for clarity in Figure 3c. We ensure that this feature is robust by performing an additional spike test (Figure S12 in Supporting Information S1). Low scattering and high absorption are expected for larger melt bodies, or melt that is not stored in fractures detectable by scattering imaging. Strong attenuation in saturated porous rocks is mostly caused by fluid flow at the mesoscopic and pore scale (Tisato & Madonna, 2012). Also, absorption has demonstrated high sensitivity to thermal gradients related to the presence of magmatic systems across subduction arcs (Vargas et al., 2019). The high-absorption body we image has a similar depth and extent as a hot, pressurized sill-complex inferred from seismicity patterns by Weinstein et al. (2017), which was suspected to have sourced the Gelai dike intrusion. Our images further show several high-absorption channels at different frequencies connecting the inferred ∼8–12 km deep sill complex to the Natron border fault, Oldoinyo Lengai and the area of the Gelai dike intrusion (Figure 3c and Figure S13 in Supporting Information S1). This could be the first evidence of a higher sensitivity of absorption imaging to small-scale thermal anomalies related to feeding and eruptive pathways.

In contrast, the core of Gelai appears as low scattering and absorbing, for example, at 6 km depth for 9 Hz (Figure 2c), which presents the lowest absorption anomaly in our models (Figures 3a and 3c). Again, we test the robustness of this feature with a spike test (Figure S14 in Supporting Information S1). Even though we can recover low absorption in the mid-frequency range, this feature is likely a combination of a low absorption feature and the focusing effects produced from wave reverberation on high-impedance contrasts (Figure S11 in Supporting Information S1; De Siena et al., 2017) and has thus to be interpreted more cautiously. Similar low-attenuation features have been previously observed at Teide volcano in Tenerife (Prudencio et al., 2015) and interpreted as old and cooled magmatic reservoirs hindering magma and fluid transport. The ages of youngest lavas erupted
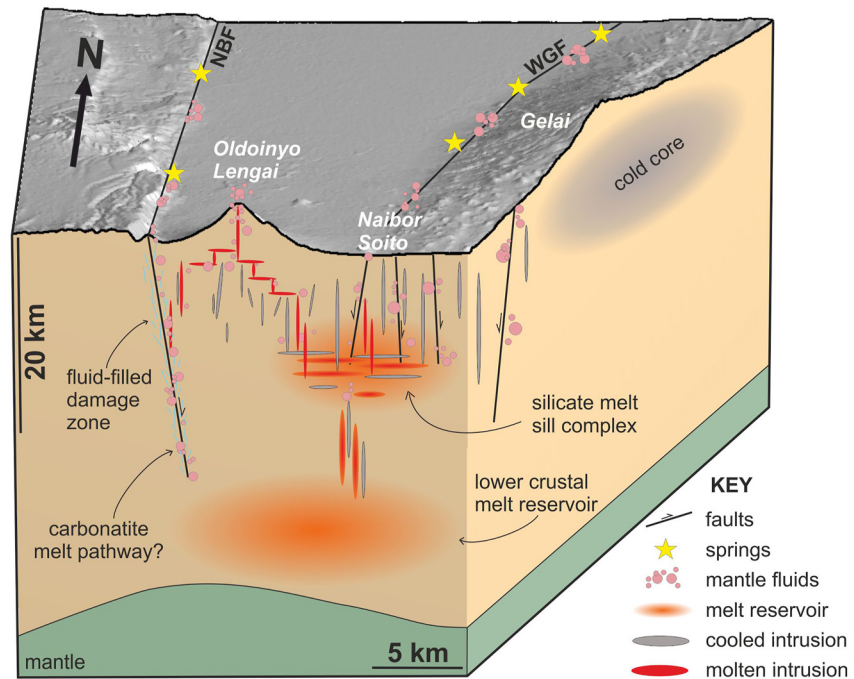
Figure 4. Conceptual illustration of the plumbing system of the Natron basin. Melt and volatiles migrate from a deeper magmatic body (Roecker et al., 2017) to a shallow silicate sill complex which may feed dike intrusions and volcanoes throughout the basin. Eruptions at Oldoinyo Lengai are additionally supplied by carbonatite melt which may be transported along the Natron border fault (NBF) which, like the Western Gelai Fault (WGF), serves as a conduit for mantle-derived volatiles.

from Gelai range from 0.95 to 1.14 Ma (Dawson et al., 1995; Mana et al., 2015; Muirhead et al., 2016). The low attenuation in the central region of the volcano may signal a cold inner core (Figure 4), confirming that the volcano is inactive, with comparatively less melt present at depth compared to surrounding regions of volcanism. At 9–12 Hz and depths ≥6 km (Figure 2c, Figures S10a and S10b in Supporting Information S1), this low absorption zone extends to Naibor Soito and crosses the top of the 2007 dike intrusion.

4.3. Fault—Plumbing System Interactions

Though we have thus far discussed the magmatic plumbing system and faults separately, our models suggest a connection between these volcano-tectonic elements, with implications for the dynamics of the rift plumbing system and the genesis of carbonatite magmatism at Oldoinyo Lengai.

The origin of carbonatite magmas at Oldoinyo is much debated, but is most often associated with liquid immiscibility at crustal pressures (de Moor et al., 2013; Fischer et al., 2009). Most interestingly, carbonatite magmas only make up a small volume fraction of erupted products, while 95% consist of silicate melts (phonolite and nephelinite; Berkesi et al., 2020; Dawson, 1962), which erupt together or separately (Keller et al., 2010). While it is beyond the scope of this paper to add to this discussion from a petrological perspective, our attenuation models suggest different melt storage and transport areas, which can be viewed in light of these different eruption products. Specifically, we image a larger melt reservoir central to the basin (Figure 3c) and a fluid-filled, highly fractured border fault (Figures 2c and 2d), suggesting at least two potential pathways for magma and fluid ascent underneath Oldoinyo Lengai (Figure 4). Carbonatite volcanoes are often found near the boundaries of cratonic lithosphere (Ernst & Bell, 2010; Muirhead et al., 2020) and in association with deep-seated faults. In the Natron basin, both volcanoes with carbonatite eruptive products, Oldoinyo Lengai and the now extinct Kerimasi, are located next to the Natron border fault, while basin volcanoes to the east (e.g., Gelai, Ketumbeine, and Naibor Soto) have no known carbonatitic volcanic products (e.g., Mana et al., 2015; Mattsson et al., 2013). Although our data suggest the plumbing system below the Naibor Soto volcanic field connects to the larger Oldoinyo Lengai plumbing system, the apparent lack of carbonatite volcanism at Naibor Soito suggests the underlying magma

system does not appear suited to either the production, or eruption, of carbonatite magmas. It is therefore plausible that carbonatite melts feeding into Oldionyo Lengai ascend along an alternative pathway, perhaps along the Natron border fault and its surrounding fracture network, which exhibits distinct HAS signature consistent with a fluid-filled fracture system (Figure 2d).

Although the connections between carbonatite volcanism and fault systems are typically based on surface observations, our seismic imaging thus supports the critical role of rift border faults for fluid and/or melt migration at depth in association with carbonatite volcanism. For example, Walter et al. (2021) recently proposed a process for fluid immiscibility and carbonatitic melt transport along pre-exisiting faults due to rapid pressure release, analog to a "pneumatic jackhammer": melt encounters the end of a pre-existing conduit where, over time, fluid overpressure causes fracturing and a sudden pressure drop followed by fluid phase separation and migration. These processes would lead to a significant damage zone around the fault, which causes scattering and absorption of seismic waves as observed at the Natron border fault and surrounding Oldoinyo Lengai (Figures 3c, 3d, and 4).

The interplay between magmatic and tectonic process in the region becomes more evident when considering the location and shape of the ~8–12 km deep sill complex. Though the exact shape and size depends on frequency (Figure S10 in Supporting Information S1), the imaged reservoir is elongated with a NE-trending long axis oblique to the rift. This shape is unusual compared to other African rift volcanoes and their underlying magma systems (Biggs et al., 2021). Obliquely oriented pre-existing structures may however play a significant role in controlling melt pathways in this region (Le Corvec et al., 2013; Muirhead & Kattenhorn, 2018; Robertson et al., 2016), and although the surface expression of faulting supports predominantly NNE-oriented faults, focal mechanism data support the presence of some NE-oriented extensional structures (Reiss et al., 2021; Weinstein et al., 2017). Furthermore, the position of the NE-oriented melt reservoir, situated between two rift segments, may be indicative of a NE-trending transfer zone that allows strain to transfer from the Natron border fault to a new segment beneath Gelai (Reiss et al., 2021; Weinstein et al., 2017). This is supported by the change in stress orientation underneath Oldoinyo Lengai and Naibor Soito, which rotates away from the regional tectonic stress field in this area (Oliva et al., 2019, 2022; Reiss et al., 2021). It may also be possible that these rift segments are linked by a series of NE-oriented structures at depth, which could facilitate the growth of an elongated magma reservoir over 10–100 kyr (Biggs & Annen, 2019).

5. Conclusions

We provide the first fine-scale 3D tomographic images of an interconnected magmatic plumbing system in a rift setting from seismic attenuation. Scattering maps highlight a highly fractured shallow crust (<6 km) in the central plumbing system, which likely reflects numerous dike intrusions since 1 Ma. The absorption models reveal a complex magmatic network in the Natron basin comprising a high-absorption melt body at 8–12 km depth and channels connecting it to Oldoinyo Lengai and dike intrusions at surface (Figure 4). The shape of this reservoir likely reflects a transfer zone between two rift segments. High scattering and absorption patterns through the primary rift faults show how fluids feed the wide-spread magmatic degassing. The Natron border fault may act as the primary pathway feeding carbonatite volcanism at Oldoinyo Lengai while silicate melts are sourced from the sill complex.

Data Availability Statement

Murat3.0 is an open-access software written in Matlab©, available at https://github.com/LucaDeSiena/MuRAT (MuRAT3.0, 2021). The data set is archived at GEOFON Data Center, https://doi.org/10.14470/4W7564850022 (Reiss & Rümpker, 2020). The final models and earthquake catalog are available in Table S1 as well as http://doi.org/10.6084/m9.figshare.20101232.

References

Akande, W. G., De Siena, L., & Gan, Q. (2019). Three-dimensional kernel-based coda attenuation imaging of caldera structures controlling the 1982–84 Campi Flegrei unrest. *Journal of Volcanology and Geothermal Research*, *381*, 273–283. https://doi.org/10.1016/j.jvolgeores.2019.06.007

Aki, K., & Chouet, B. (1975). Origin of coda waves: Source, attenuation, and scattering effects. *Journal of Geophysical Research*, *80*(23), 3322–3342. https://doi.org/10.1029/jb080i023p03322

Albaric, J., Deverchere, J., Perrot, J., Jakovlev, A., & Deschamps, A. (2014). Deep crustal earthquakes in North Tanzania, East Africa: Interplay between tectonic and magmatic processes in an incipient rift. *Geochemistry, Geophysics, Geosystems*, *15*(2), 374–394. https://doi.org/10.1002/2013GC005027

Aulbach, S., Rudnick, R. L., & McDonough, W. F. (2011). Evolution of the lithospheric mantle beneath the East African Rift in Tanzania and its potential signatures in rift magmas. *The Geological Society of America Bulletin*, *478*, 105–125.

Baer, G., Hamiel, Y., Shamir, G., & Nof, R. (2008). Evolution of a magma driven earthquake swarm and triggering of the nearby Oldoinyo Lengai eruption, as resolved by InSAR, ground observations and elastic modeling, East African Rift, 2007. *Earth and Planetary Science Letters*, *272*(1–2), 339–352. https://doi.org/10.1016/j.epsl.2008.04.052

Berkesi, M., Bali, E., Bodnar, R. J., Szabó, Á., & Guzmics, T. (2020). Carbonatite and highly peralkaline nephelinite melts from Oldoinyo Lengai Volcano, Tanzania: The role of natrite-normative fluid degassing. *Gondwana Research*, *85*, 76–83. https://doi.org/10.1016/j.gr.2020.03.013

Biggs, J., & Annen, C. (2019). The lateral growth and coalescence of magma systems. *Philosophical Transactions of the Royal Society A*, *377*(2139), 20180005. https://doi.org/10.1098/rsta.2018.0005

Biggs, J., Anthony, E. Y., & Ebinger, C. J. (2009). Multiple inflation and deflation events at Kenyan volcanoes, East African Rift. *Geology*, *37*(11), 979–982. https://doi.org/10.1130/g30133a.1

Biggs, J., Ayele, A., Fischer, T. P., Fontijn, K., Hutchison, W., Kazimoto, E., et al. (2021). Volcanic activity and hazard in the East African Rift Zone. *Nature Communications*, *688*(1), 2041–1723. https://doi.org/10.1038/s41467-021-27166-y

Biggs, J., Chivers, M., & Hutchinson, M. C. (2013). Surface deformation and stress interactions during the 2007–2010 sequence of earthquake, dyke intrusion and eruption in northern Tanzania. *Geophysical Journal International*, *195*(1), 16–26. https://doi.org/10.1093/gji/ggt226

Buck, W. R. (2004). Consequences of asthenospheric variability on continental rifting. In *Rheology and Deformation of the Lithosphere at Continental Margins: MARGINaibor Soito Theoretical and Experimental Earth Science Series* (pp. 1–30). Columbia University Press.

Calais, E., d'Oreye, N., Albaric, J., Deschamps, A., Delvaux, D., Déverchère, J., et al. (2008). Strain accommodation by slow slip and dyking in a youthful continental rift, East Africa. *Nature*, *456*(7223), 783–787. https://doi.org/10.1038/nature07478

Calvet, M., Sylvander, M., Margerin, L., & Villaseñor, A. (2013). Spatial variations of seismic attenuation and heterogeneity in the Pyrenees: Coda Q and peak delay time analysis. *Tectonophysics*, *608*, 428–439. https://doi.org/10.1016/j.tecto.2013.08.045

Dawson, J. (1962). Sodium carbonate lavas from Oldoinyo Lengai, Tanganyika. *Nature*, *195*(4846), 1075–1076. https://doi.org/10.1038/1951075a0

Dawson, J. B., Keller, J., & Nyamweru, C. (1995). Historic and recent eruptive activity of Oldoinyo Lengai. In K. Bell & J. Keller (Eds.), *Carbonatite volcanism: Oldoinyo Lengai and the petrogenesis of natrocarbonatites*. *IAVCEI Proceedings of Volcanology* (Vol. 4, pp. 4–22). Springer.

Del Pezzo, E., De La Torre, A., Bianco, F., Ibanez, J., Gabrielli, S., & De Siena, L. (2018). Numerically calculated 3D space-weighting functions to image crustal volcanic structures using diffuse coda waves. *Geosciences*, *8*(5), 175. https://doi.org/10.3390/geosciences8050175

Del Pezzo, E., & Ibáñez, J. M. (2020). Seismic coda-waves imaging based on sensitivity kernels calculated using an heuristic approach. *Geosciences*, *10*(8), 304. https://doi.org/10.3390/geosciences10080304

de Moor, M., Fischer, T. P., King, P. L., Botcharnikov, R. E., Hervig, R. L., Hilton, D. R., et al. (2013). Volatile-rich silicate melts from Oldoinyo Lengai volcano (Tanzania): Implications for carbonatite genesis and eruptive behavior. *Earth and Planetary Science Letters*, *361*, 379–390. https://doi.org/10.1016/j.epsl.2012.11.006

De Siena, L., Amoruso, A., Pezzo, E. D., Wakeford, Z., Castellano, M., & Crescentini, L. (2017). Space-weighted seismic attenuation mapping of the aseismic source of Campi Flegrei 1983–1984 unrest. *Geophysical Research Letters*, *44*(4), 1740–1748.

De Siena, L., Calvet, M., Watson, K. J., Jonkers, A., & Thomas, C. (2016). Seismic scattering and absorption mapping of debris flows, feeding paths, and tectonic units at Mount St. Helens volcano. *Earth and Planetary Science Letters*, *442*, 21–31. https://doi.org/10.1016/j.epsl.2016.02.026

Ebinger, C., & Casey, M. (2001). Continental breakup in magmatic provinces: An Ethiopian example. *Geology*, *29*(6), 527–530. https://doi.org/10.1130/0091-7613(2001)029<0527:cbimpa>2.0.co;2

Ebinger, C., Djomani, Y. P., Mbede, E., Foster, A., & Dawson, J. B. (1997). Rifting Archaean lithosphere: The Eyasi–Manyara–Natron rifts, East Africa. *Journal of the Geological Society*, *154*(6), 947–960. https://doi.org/10.1144/gsjgs.154.6.0947

Ernst, R. E., & Bell, K. (2010). Large igneous provinces (LIPs) and carbonatites. *Mineralogy and Petrology*, *98*(1), 55–76. https://doi.org/10.1007/s00710-009-0074-1

Fischer, T. P., Burnard, P., Marty, B., Hilton, D. R., Furi, E., Palhol, F., et al. (2009). Upper-mantle volatile chemistry at Oldoinyo Lengai volcano and the origin of carbonatites. *Nature*, *459*(7243), 77–80. https://doi.org/10.1038/nature07977

Foster, A., Ebinger, C., Mbede, E., & Rex, D. (1997). Tectonic development of the northern Tanzanian sector of the East African Rift System. *Journal of the Geological Society*, *154*(4), 689–700. https://doi.org/10.1144/gsjgs.154.4.0689

Gabrielli, S., De Siena, L., Napolitano, F., & Del Pezzo, E. (2020). Understanding seismic path biases and magmatic activity at Mount St Helens volcano before its 2004 eruption. *Geophysical Journal International*, *222*(1), 169–188. https://doi.org/10.1093/gji/ggaa154

Jones, J. R., Stamps, D. S., Wauthier, C., Saria, E., & Biggs, J. (2019). Evidence for slip on a border fault triggered by magmatic processes in an immature continental rift. *Geochemistry, Geophysics, Geosystems*, *20*(5), 2515–2530. https://doi.org/10.1029/2018gc008165

Keir, D., Ebinger, C., Daly, E., Stuart, G., Maguire, P., & Ayele, A. (2006). Strain accommodation by magmatism and faulting as rifting proceeds to breakup: Seismicity of the northern Ethiopian rift. *Journal of Geophysical Research*, *111*(B5), B05314. https://doi.org/10.1029/2005JB003748

Keller, J., Klaudius, J., Kervyn, M., Ernst, G. G. J., & Mattsson, H. B. (2010). Fundamental changes in the activity of the natrocarbonatite volcano Oldoinyo Lengai, Tanzania. *Bulletin of Volcanology*, *72*(8), 893–912. https://doi.org/10.1007/s00445-010-0371-x

Kervyn, M., Ernst, G. G. J., Keller, J., Vaughan, G., Klaudius, J., Pradal, E., et al. (2010). Fundamental changes in the activity of the natrocarbonatite volcano Oldoinyo Lengai, Tanzania. II. Eruptive behavior. *Bulletin of Volcanology*, *72*(8), 913–931. https://doi.org/10.1007/s00445-010-0360-0

Le Corvec, N., Spörli, K. B., Rowland, J., & Lindsay, J. (2013). Spatial distribution and alignments of volcanic centers: Clues to the formation of monogenetic volcanic fields. *Earth-Science Reviews*, *124*, 96–114. https://doi.org/10.1016/j.earscirev.2013.05.005

Lee, H., Fischer, T. P., Muirhead, J. D., Ebinger, C. J., Kattenhorn, S. A., Sharp, Z. D., et al. (2017). Incipient rifting accompanied by the release of subcontinental lithospheric mantle volatiles in the Magadi and Natron basin, East Africa. *Journal of Volcanology and Geothermal Research*, *346*, 118–133. https://doi.org/10.1016/j.jvolgeores.2017.03.017

Lee, H., Muirhead, J. D., Fischer, T. P., Ebinger, C. J., Kattenhorn, S. A., Sharp, Z. D., & Kianji, G. (2016). Massive and prolonged deep carbon emissions associated with continental rifting. *Nature Geoscience*, *9*(2), 145–149. https://doi.org/10.1038/ngeo2622

Le Gall, B., Nonnotte, P., Rolet, J., Benoit, M., Guillou, H., Mousseau-Nonnotte, M., et al. (2008). Rift propagation at craton margin. Distribution of faulting and volcanism in the North Tanzanian Divergence (East Africa) during Neogene times. *Tectonophysics*, *448*(1–4), 1–19. https://doi.org/10.1016/j.tecto.2007.11.005

Mana, S., Furman, T., Turrin, B. D., Feigenson, M. D., & Swisher, C. C. (2015). Magmatic activity across the East African North Tanzanian divergence zone. *Journal of the Geological Society*, *172*(3), 368–389. https://doi.org/10.1144/jgs2014-072

Marzen, R. E., Shillington, D. J., Lizarralde, D., Knapp, J. H., Heffner, D. M., Davis, J. K., & Harder, S. H. (2020). Limited and localized magmatism in the Central Atlantic Magmatic Province. *Nature Communications*, *11*(1), 3397–3398. https://doi.org/10.1038/s41467-020-17193-6

Mattsson, H. B., Nandedkar, R. H., & Ulmer, P. (2013). Petrogenesis of the melilititic and nephelinitic rock suites in the Lake Natron–Engaruka monogenetic volcanic field, northern Tanzania. *Lithos*, *179*, 175–192. https://doi.org/10.1016/j.lithos.2013.07.012

Mayor, J., Calvet, M., Margerin, L., Vanderhaeghe, O., & Traversa, P. (2016). Crustal structure of the Alps as seen by attenuation tomography. *Earth and Planetary Science Letters*, *439*, 71–80. https://doi.org/10.1016/j.epsl.2016.01.025

Moore, D. E., & Rymer, M. J. (2007). Talc-bearing serpentinite and the creeping section of the San Andreas fault. *Nature*, *448*(7155), 795–797.

Muirhead, J. D., Fischer, T. P., Oliva, S. J., Laizer, A., van Wijk, J., Currie, C. A., et al. (2020). Displaced cratonic mantle concentrates deep carbon during continental rifting. *Nature*, *582*(7810), 67–72. https://doi.org/10.1038/s41586-020-2328-3

Muirhead, J. D., & Kattenhorn, S. A. (2018). Activation of preexisting transverse structures in an evolving magmatic rift in East Africa. *Journal of Structural Geology*, *106*, 1–18. https://doi.org/10.1016/j.jsg.2017.11.004

Muirhead, J. D., Kattenhorn, S. A., & Le Corvec, N. (2015). Varying styles of magmatic strain accommodation across the East African Rift. *Geochemistry, Geophysics, Geosystems*, *16*(8), 2–2795. https://doi.org/10.1002/2015gc005918

Muirhead, J. D., Kattenhorn, S. A., Lee, H., Mana, S., Turrin, B. D., Fischer, T. P., et al. (2016). Evolution of upper crustal faulting assisted by magmatic volatile release during early-stage continental rift development in the East African Rift. *Geosphere*, *12*(6), 1670–1700. https://doi.org/10.1130/ges01375.1

MuRAT 3.0. (2021). Original version [Software]. LucaDeSiena/MuRAT. Retrieved from https://github.com/LucaDeSiena/MuRAT

Napolitano, F., De Siena, L., Gervasi, A., Guerra, I., Scarpa, R., & La Rocca, M. (2020). Scattering and absorption imaging of a highly fractured fluid-filled seismogenetic volume in a region of slow deformation. *Geoscience Frontiers*, *11*(3), 989–998. https://doi.org/10.1016/j.gsf.2019.09.014

Oliva, S. J., Ebinger, C. J., Rivalta, E., Williams, C. A., Wauthier, C., & Currie, C. A. (2022). State of stress and stress rotations: Quantifying the role of surface topography and subsurface density contrasts in magmatic rift zones (Eastern Rift, Africa). *Earth and Planetary Science Letters*, *584*, 117478. https://doi.org/10.1016/j.epsl.2022.117478

Oliva, S. J., Ebinger, C. J., Wauthier, C., Muirhead, J. D., Roecker, S. W., Rivalta, E., & Heimann, S. (2019). Insights into fault-magma interactions in an early-stage continental rift from source mechanisms and correlated volcano-tectonic earthquakes. *Geophysical Research Letters*, *46*(4), 2065–2074. https://doi.org/10.1029/2018gl080866

Prudencio, J., Ibáñez, J., Del Pezzo, E., Martí, J., García-Yeguas, A., & De Siena, L. (2015). 3D attenuation tomography of the volcanic island of Tenerife (Canary Islands). *Surveys in Geophysics*, *36*(5), 693–716. https://doi.org/10.1007/s10712-015-9333-3

Prudencio, J., Manga, M., & Taira, T. (2018). Subsurface structure of Long Valley Caldera imaged with seismic scattering and intrinsic attenuation. *Journal of Geophysical Research: Solid Earth*, *123*(7), 5987–5999. https://doi.org/10.1029/2017jb014986

Reiss, M. C., Muirhead, J. D., Laizer, A. S., Link, F., Kazimoto, E. O., Ebinger, C. J., & Rümpker, G. (2021). The impact of complex volcanic plumbing on the nature of Seismicity in the developing Magmatic Natron Rift, Tanzania. *Frontiers of Earth Science*, *8*, 609805. https://doi.org/10.3389/feart.2020.609805

Reiss, M. C., & Rümpker, G. (2020). SEISVOL - Seismic and infrasound networks to study the volcano Oldoinyo Lengai [Dataset]. GFZ Data Services. https://doi.org/10.14470/4W7564850022

Reyners, M., Eberhart-Phillips, D., & Stuart, G. (2007). The role of fluids in lower-crustal earthquakes near continental rifts. *Nature*, *446*(7139), 1075–1078. https://doi.org/10.1038/nature05743

Robertson, E. A. M., Biggs, J., Cashman, K. V., Floyd, M. A., & Vye-Brown, C. (2016). Influence of regional tectonics and pre-existing structures on the formation of elliptical calderas in the Kenyan Rift. *Geological Society, London, Special Publications*, *420*(1), 43–67. https://doi.org/10.1144/SP420.12

Roecker, S., Ebinger, C., Tiberi, C., Mulibo, G., Wambura, F., Mtelela, K., et al. (2017). Subsurface images of the Eastern Rift, Africa, from the joint inversion of body waves, surface waves and gravity: Investigating the role of fluids in early-stage continental rifting. *Geophysical Journal International*, *210*(2), 931–950. https://doi.org/10.1093/gji/ggx220

Rowland, J. V., Baker, E., Ebinger, C. J., Keir, D., Kidane, T., Biggs, J., et al. (2007). Fault growth at a nascent slow-spreading ridge: 2005 Dabbahu rifting episode, Afar. *Geophysical Journal International*, *171*(3), 1226–1246. https://doi.org/10.1111/j.1365-246x.2007.03584.x

Rubin, A. M., & Pollard, D. D. (1988). Dike-induced faulting in rift zones of Iceland and Afar. *Geology*, *16*(5), 413–417. https://doi.org/10.1130/0091-7613(1988)016<0413:difirz>2.3.co;2

Saria, E., Calais, E., Stamps, D. S., Delvaux, D., & Hartnady, C. J. H. (2014). Present-day kinematics of the East African Rift. *Journal of Geophysical Research: Solid Earth*, *119*(4), 3584–3600. https://doi.org/10.1002/2013jb010901

Shapiro, N. M., Campillo, M., Margerin, L., Singh, S. K., Kostoglodov, V., & Pacheco, J. (2000). The energy partitioning and the diffusive character of the seismic coda. *Bulletin of the Seismological Society of America*, *90*(3), 655–665. https://doi.org/10.1785/0119990021

Sherrod, D. R., Magigita, M. M., & Kwelwa, S. (2013). Geologic map of Oldonyo Lengai (Oldoinyo Lengai) and surroundings, Arusha Region, United Republic of Tanzania. *U.S. Geological Survey Report 2013-1306*, 65.

Shito, A., Matsumoto, S., Ohkura, T., Shimizu, H., Sakai, S., Iio, Y., et al. (2020). 3-D intrinsic and scattering seismic attenuation structures beneath Kyushu, Japan. *Journal of Geophysical Research: Solid Earth*, *125*(8), e2019JB018742. https://doi.org/10.1029/2019jb018742

Sibson, R. H. (2000). Fluid involvement in normal faulting. *Journal of Geodynamics*, *29*(3–5), 469–499. https://doi.org/10.1016/s0264-3707(99)00042-3

Takahashi, T., Sato, H., Nishimura, T., & Obara, K. (2007). Strong inhomogeneity beneath Quaternary volcanoes revealed from the peak delay analysis of S-wave seismograms of microearthquakes in northeastern Japan. *Geophysical Journal International*, *168*(1), 90–99. https://doi.org/10.1111/j.1365-246x.2006.03197.x

Thybo, H., & Nielsen, C. A. (2009). Magma-compensated crustal thinning in continental rift zones. *Nature*, *457*(7231), 873–876. https://doi.org/10.1038/nature07688

Tiberi, C., Gautier, S., Ebinger, C., Roecker, S., Plasman, M., Albaric, J., et al. (2019). Lithospheric modification by extension and magmatism at the craton-orogenic boundary: North Tanzania Divergence, East Africa. *Geophysical Journal International*, *216*(3), 1693–1710. https://doi.org/10.1093/gji/ggy521

Tisato, N., & Madonna, C. (2012). Attenuation at low seismic frequencies in partially saturated rocks: Measurements and description of a new apparatus. *Journal of Applied Geophysics*, *86*, 44–53. https://doi.org/10.1016/j.jappgeo.2012.07.008

Tisato, N., Quintal, B., Chapman, S., Podladchikov, Y., & Burg, J.-P. (2015). Bubbles attenuate elastic waves at seismic frequencies: First experimental evidence. *Geophysical Research Letters*, *42*(10), 3880–3887. https://doi.org/10.1002/2015GL063538

Trippanera, D., Ruch, J., Passone, L., & Jónsson, S. (2019). Structural mapping of dike-induced faulting in Harrat Lunayyir (Saudi Arabia) by using high resolution drone imagery. *Frontiers of Earth Science*, *7*, 168. https://doi.org/10.3389/feart.2019.00168

Vargas, C. A., Ochoa, L. H., & Caneva, A. (2019). Estimation of the thermal structure beneath the volcanic arc of the Northern Andes by coda wave attenuation tomography. *Frontiers of Earth Science*, *7*, 208. https://doi.org/10.3389/feart.2019.00208

Walter, B. F., Giebel, R. J., Steele-MacInnis, M., Marks, M. A. W., Kolb, J., & Markl, G. (2021). Fluids associated with carbonatitic magmatism: A critical review and implications for carbonatite magma ascent. *Earth-Science Reviews*, *215*, 103509. https://doi.org/10.1016/j.earscirev.2021.103509

Wegler, U., & Lühr, B. G. (2001). Scattering behaviour at Merapi volcano (Java) revealed from an active seismic experiment. *Geophysical Journal International*, *145*(3), 579–592. https://doi.org/10.1046/j.1365-246x.2001.01390.x

Weinstein, A., Oliva, S. J., Ebinger, C. J., Roecker, S., Tiberi, C., Aman, M., et al. (2017). Fault-magma interactions during early continental rifting: Seismicity of the Magadi-Natron-Manyara basins, Africa. *Geochemistry, Geophysics, Geosystems*, *18*(10), 3662–3686. https://doi.org/10.1002/2017GC007027

Zhang, T., Sens-Schönfelder, C., & Margerin, L. (2021). Sensitivity kernels for static and dynamic tomography of scattering and absorbing media with elastic waves: A probabilistic approach. *Geophysical Journal International*, *225*(3), 1824–1853. https://doi.org/10.1093/gji/ggab048

Zieger, T., Sens-Schönfelder, C., Ritter, J. R., Lühr, B., & Dahm, T. (2016). P-wave scattering and the distribution of heterogeneity around Etna volcano. *Annals of Geophysics*, *59*(4). https://doi.org/10.4401/ag-7085

References From the Supporting Information

Calvet, M., & Margerin, L. (2013). Lapse-time dependence of coda Q: Anisotropic multiple-scattering models and application to the Pyrenees. *Bulletin of the Seismological Society of America*, *103*(3), 1993–2010. https://doi.org/10.1785/0120120239

Gazzola, S., Hansen, P. C., & Nagy, J. G. (2019). IR Tools: A MATLAB package of iterative regularization methods and large-scale test problems. *Numerical Algorithms*, *81*(3), 773–811. https://doi.org/10.1007/s11075-018-0570-7

Havskov, J., Sørensen, M. B., Vales, D., Özyazıcıoglu, M., Sanchez, G., & Li, B. (2016). Coda Q in different tectonic areas, influence of processing parameters. *Bulletin of the Seismological Society of America*, *106*(3), 956–970. https://doi.org/10.1785/0120150359

Hennino, R., Trégourès, N., Shapiro, N. M., Margerin, L., Campillo, M., van Tiggelen, B. A., & Weaver, R. L. (2001). Observation of equipartition of seismic waves. *Physical Review Letters*, *86*(15), 3447–3450. https://doi.org/10.1103/physrevlett.86.3447

Margerin, L. (2017). Breakdown of equipartition in diffuse fields caused by energy leakage. *The European Physical Journal - Special Topics*, *226*(7), 1353–1370. https://doi.org/10.1140/epjst/e2016-60165-6

Plasman, M., Tiberi, C., Ebinger, C., Gautier, S., Albaric, J., Peyrat, S., et al. (2017). Lithospheric low-velocity zones associated with a magmatic segment of the Tanzanian Rift, East Africa. *Geophysical Journal International*, *210*(1), 465–481. https://doi.org/10.1093/gji/ggx177

Zenonos, A., De Siena, L., Widiyantoro, S., & Rawlinson, N. (2019). P and S wave travel time tomography of the SE Asia-Australia collision zone. *Physics of the Earth and Planetary Interiors*, *293*, 106267. https://doi.org/10.1016/j.pepi.2019.05.010